International Journal of Thermophysics, Vol. 28, No. 2, April 2007 (© 2007)
DOI: 10.1007/s10765-007-0178-y

Thermophysical Properties of a Refrigerant Mixture of R365mfc (1,1,1,3,3-Pentafluorobutane) and Galden® HT 55 (Perfluoropolyether)

A. P. Fröba,[1,2,3] H. Kremer,[2] A. Leipertz,[1,2] F. Flohr,[4] and C. Meurer[4]

This work presents a comprehensive experimental study of various thermophysical properties of an azeotropic refrigerant mixture of 65 mass% R365mfc (1,1,1,3,3-pentafluorobutane) and 35 mass% Galden® HT 55 (perfluoropolyether). Light scattering from bulk fluids has been applied for measuring both the thermal diffusivity and the speed of sound in the liquid and vapor phases under saturation conditions, between 293 K and the liquid–vapor critical point at 450.7 K. Furthermore, the speed of sound has been measured for the superheated-vapor phase along nine isotherms, between 393 and 523 K and up to a maximum pressure of about 2.5 MPa. For temperatures between 253 and 413 K, light scattering by surface waves on a horizontal liquid–vapor interface has been used for simultaneous determination of the surface tension and kinematic viscosity of the liquid phase. With light scattering techniques, uncertainties of less than ±2.0%, ±0.5%, ±1.5%, and ±1.5% have been achieved for the thermal diffusivity, sound speed, kinematic viscosity, and surface tension, respectively. In addition to vapor-pressure measurements between 304 and 448 K, the density was measured between 273 and 443 K using a vibrating-tube method. Here, measurements have been performed in the compressed- and saturated-liquid phases with uncertainties of ±0.3% and ±0.1%, respectively, as well as for the superheated vapor up to a maximum pressure of about 3 MPa with an uncertainty between ±0.3% and ±3%. Critical-point parameters were derived by combining the data obtained by different techniques.

[1] Lehrstuhl für Technische Thermodynamik (LTT), Friedrich-Alexander-Universität Erlangen-Nürnberg, Am Weichselgarten 8, D-91058 Erlangen, Germany.
[2] ESYTEC Energie- und Systemtechnik GmbH, Am Weichselgarten 6, D-91058 Erlangen, Germany.
[3] To whom correspondence should be addressed. E-mail: apf@ltt.uni-erlangen.de
[4] SOLVAY Fluor GmbH, Hans-Böckler-Allee 20, D-30173 Hannover, Germany.

KEY WORDS: density; Galden® HT 55; 1,1,1,3,3-pentafluorobutane; perfluoropolyether; R365mfc; Solkatherm® SES36; sound speed; surface tension; thermal diffusivity; vapor pressure; viscosity.

1. INTRODUCTION

The efficient use of energy is increasingly becoming a focus of politics as a result of the increasing consumption of energy throughout the world. In this context, emissions associated with the consumption of fossil energy sources have to be minimized due to their contribution to air pollution and to the greenhouse effect. One approach for an economical and ecological use of such energy sources is to utilize the waste heat from many different processes, e.g., by installing high temperature heat-pump systems in combined heat and power plants. Another approach is to exploit natural energy sources, e.g., in geothermal or solar-thermal power plants. One key component for the efficient utilization of these energy sources is the working fluid.

A newly developed working fluid particularly suitable for the abovementioned applications is an azeotropic mixture composed of 65 mass% R365mfc (1,1,1,3,3-pentafluorobutane) and 35 mass% Galden® HT 55 (perfluoropolyether). This multicomponent mixture, which is named in the following by its trade name, Solkatherm® SES36, contains through the pseudo-component Galden® HT 55 more than eight different types of perfluoropolyethers (PFPE) with low boiling points. The total share of PFPE is, however, characteristic of a selected batch of Galden® HT 55, for which the characteristics of SES36 were obtained. This nonflammable mixture with low toxicity offers, due to its higher vapor density in comparison to steam or other common working fluids for high-temperature applications, better heat transfer performance for temperatures lower than 400°C. In general, another area of application of such a working fluid is its use as a heat transfer fluid, e.g., for the efficient cooling of electrical components.

For SES36, neither equilibrium data nor transport properties can be found in the literature. It is the major aim of this work to contribute to a comprehensive and reliable database for this newly developed working fluid. In the present article, first, the methodological principles and experimental conditions for the measurement techniques used for the determination of vapor pressure, density, thermal diffusivity, sound speed, viscosity, and surface tension are briefly reviewed. Then, the experimental results are presented.

2. METHODS AND EXPERIMENTAL CONDITIONS

For all experiments, the same SES36 sample has been used, where the uncertainty in the composition regarding R365mfc and Galden® HT 55 can be estimated to be ±0.1% for each component. For the pseudo-component Galden® HT 55, a mean molar mass of about $343\,g \cdot mol^{-1}$ can be found for the selected batch. On the basis of the molar mass of $148.076\,g \cdot mol^{-1}$ for R365mfc, a molar mass of $184.85\,g \cdot mol^{-1}$ for SES36 is obtained. According to the specification of the manufacturer (Solvay Fluor GmbH, Hannover), the sample had a purity of $\geqslant$99.7% and was used without further purification.

2.1. Vapor-Pressure Measurement

The determination of the vapor pressure of SES36 was carried out with the same sample cell used for the measurement of thermal diffusivity and speed of sound by "conventional" dynamic light scattering; see Section 2.3. For the measurement of the pressure, a digital pressure reference (RPM1, Desgranges & Huot) was used, consisting of a quartz pressure transducer with a resolution of 1 Pa and an absolute uncertainty of less than ±1.5 kPa. The pressure transducer was connected with the measurement cell via a cooling capillary. The actual temperature in the sample cell, which was placed in an insulated housing, was regulated through resistance heating with a long-term stability better than ±2 mK. The vessel temperature was measured with a calibrated 25 Ω platinum resistance probe integrated into the main body of the measuring cell, with a resolution of 0.1 mK, using an ac bridge (MKT 25, Anton Paar). The absolute uncertainty of the temperature measurement was less than ±5 mK. A separate filling system was used to degas the sample, as well as to flush and evacuate the measurement cell with the help of a vacuum pump. The refrigerant sample was filled from the liquid phase into the evacuated measuring cell system. For attributing the vapor pressure to the corresponding temperature when approaching mechanical and thermal equilibrium, the long-term stability of the measuring cell system was better than ±0.1 kPa. Taking into account all individual error sources, a total uncertainty of about ±2 kPa can be estimated for the present vapor-pressure measurements.

2.2. Vibrating-Tube Method for Density

For the density measurements, the vibrating-tube method was used, where a hollow U-shaped tube is forced into harmonic oscillation. The

period of oscillation τ is dependent on the density ρ of the sample in the tube. Therefore, by measuring the period of oscillation, the density is calculated;

$$\rho = A\tau^2 - B, \tag{1}$$

where the apparatus constants A and B have to be evaluated using two samples of known density.

For the density meter (DMA 5000, Anton Paar) used to determine the liquid density under saturation conditions in the temperature range from 273 to 363 K, a reference oscillator is built into the measuring cell, which eliminates long-term drift, and only one adjustment at 20°C is sufficient to reach a high accuracy for the whole measuring temperature range. The DMA 5000 allows a full-range viscosity correction, whereby all viscosity-related errors inherent to all known types of oscillating U-tube density meters are automatically eliminated. The temperature of the U-tube is controlled within ±1 mK using Peltier elements and measured by a high-precision platinum resistance probe with an uncertainty of ±10 mK. The DMA 5000 was calibrated with standard water and dry air. Before measuring the saturated-liquid density, the U-tube was evacuated. Subsequently, the sample was filled from the liquid phase into the U-tube of the density meter.

An external measuring cell (DMA 602, Anton Paar) was used to determine the density in the compressed-liquid and superheated-vapor phases for temperatures between 373 and 448 K and 347 and 448 K, respectively. Measurements in the compressed-liquid and superheated-vapor phases were performed for pressures extending from those close to the saturation line up to about 4 MPa and down to about 0.1 MPa, respectively. A schematic diagram of the external measuring cell and its peripheral equipment is given in Fig. 1. The temperature of the external measuring cell with a long-term stability of better than ±5 mK was regulated using a lab thermostat. The temperature inside the vibrating U-tube was determined with a calibrated 100 Ω platinum resistance probe with a resolution of 0.25 mK using an ac bridge (MKT 100, Anton Paar). The uncertainty of the absolute temperature measurement was less than ±20 mK. For the measurement of the pressure, the same digital pressure reference (RPM1, Desgranges & Huot) described for the measurement of the vapor pressure in Section 2.1 was used. The pressure transducer was also connected by a cooling capillary to the measurement system and an uncertainty of less than ±1.5 kPa can be stated for the pressure measurements over the complete pressure range. The long-term stability of the measurement system was better than ±1 and ±10 kPa for the determination of

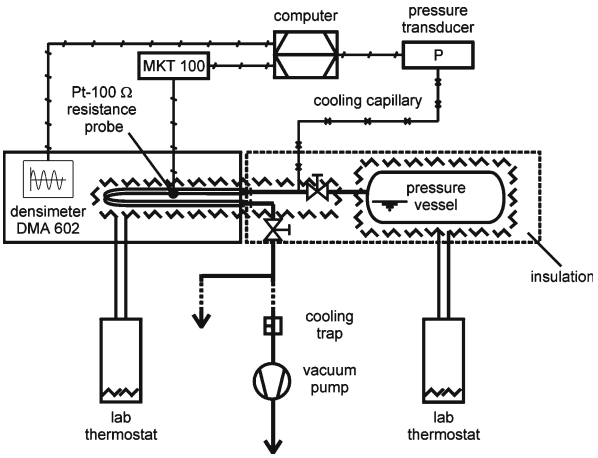

Fig. 1. External measuring cell (DMA 602, Anton Paar) and its peripheral equipment for density determination.

the density in the superheated-vapor and compressed-liquid phases, respectively.

The densimeter was calibrated with 1,1-dichloro-2,2,2-trifluoroethane (R123) and nitrogen (N_2). For the investigation of SES36 and the calibration procedure with R123, the densimeter was filled from a thermostatted pressure vessel connected via a precision metering valve to the inlet of the U-tube. Prior to loading the densimeter with R123 or SES36, the sample was degassed and the complete measuring system was evacuated. In the thermostatted pressure vessel, however, SES36 or R123, existed always in the two-phase region. Through the adjustment of the temperature of the thermostatted pressure vessel at least 10 K below or above the desired temperature inside the U-tube, the thermodynamic state was fixed to be either in the superheated-vapor or in the compressed-liquid phase, respectively. For calibration of the densimeter in the low-density region, N_2 was filled at or close to room temperature directly from the original sample cylinder after prior evacuation of the measuring system. For all fluids, the pressure inside the measuring system could be adjusted by the precision metering valve at the inlet of the U-tube, as well as by an additional one situated at its outlet.

The apparatus constants A and B in Eq. (1) were determined by measuring the temperature and pressure dependences of the tube's oscillating period τ when it was filled with N_2 and R123. The density measurements for SES36 in the superheated-vapor phase are based on the calibration of the densimeter with N_2 and R123 over the temperature ranges of 323–448

and 373–448 K, respectively, and over the pressure ranges of 0.1–3.5 and 0.1–2.5 MPa, respectively. The measurements in the compressed-liquid phase are also based on the above-stated calibration with N_2. In addition, the calibration was performed with R123 in its compressed-liquid state over the temperature and pressure ranges from 373 to 448 K and from 1 to 4.1 MPa. Some state points of SES36 in the compressed-liquid phase correspond to the two-phase region of R123. In this case, the parameters A and B of Eq. (1) were obtained by an adequate extrapolation.

For the calibration, the densities of N_2 and R123 were taken from the standard reference database program REFPROP [1], where uncertainties of 0.02% and 0.1%, respectively, are reported. For estimation of the overall uncertainty, all individual error contributions have been taken into account, including pressure and temperature instabilities. The results for the superheated-vapor phase are strongly influenced by the uncertainty of the pressure measurement and the pressure instability. The overall uncertainty increases from ±0.3% at 2.5 MPa to ±3% at 0.1 MPa. For all density data in the compressed-liquid phase, an overall uncertainty of less than ±0.3% can be stated. The present measurements and the uncertainty analysis have been checked by measuring the density of sulfur hexafluoride (SF_6) on the basis of the above-described calibration procedure. For temperatures between 373 and 448 K and for pressures from 0.1 to 3 MPa, the average absolute deviation of our density data for SF_6 and those calculated by REFPROP [1] is smaller than 1.3%.

2.3. Thermal Diffusivity and Sound Speed by Light Scattering from Bulk Fluids

The principle of dynamic light scattering (DLS) for the determination of thermal diffusivity and sound speed is given in detail elsewhere; see, e.g., Refs. 2–5. Here, only the essential features are repeated and some attention is given to the analysis of the thermal diffusivity in a multicomponent mixture as it is relevant for this work.

When a fluid sample in macroscopic thermodynamic equilibrium is irradiated by coherent laser light, light scattered from the sample can be observed in all directions. The underlying scattering process is governed by microscopic fluctuations of temperature (or entropy), of pressure, and of species concentration in mixtures. The relaxations of these statistical fluctuations follow the same rules that are valid for the relaxation of macroscopic systems. The decay of temperature fluctuations is governed by the thermal diffusivity. Pressure fluctuations in fluids are moving with the sound speed, and their decay is governed by the sound attenuation. In a fluid mixture, the decay of concentration fluctuations is related to mass

diffusivities in a more or less complex way, depending on the number of single species. This is represented in the simplest case of a binary fluid mixture by the binary diffusion coefficient. In light scattering experiments, the above-mentioned equalization processes result in a temporal modulation of the scattered light intensity. Information about these processes can be derived through a temporal analysis of the scattered light intensity using photon correlation spectroscopy (PCS).

While the measurement of the thermal diffusivity in pure fluids is basically a straightforward task, this is clearly more difficult in fluid mixtures. Even in the simplest case of a binary fluid mixture, neglecting the pressure fluctuations and applying heterodyne conditions, where the scattered light is superimposed with stronger coherent reference light, the correlation function takes the form of a sum of two exponentials [4, 5]. While the interpretation of DLS experiments on binary fluid mixtures can be regarded to be state of the art, for ternary and multicomponent mixtures, a corresponding interpretation is either still the subject of current research activities [6] or completely lacking regarding the signals observable due to concentration fluctuations. Whether it is possible to determine signals from concentration fluctuations is mainly governed by the relative difference of the refractive indices of the mixture components and their concentrations. In this work, however, for heterodyne conditions, the time-dependent intensity correlation function for the analysis of the temperature fluctuations is described by

$$G^{(2)}(\tau) = A + B\,\exp(-\tau/\tau_{C_t}) + D\tau \tag{2}$$

where through the linear term, the concentration fluctuations are treated as a low-amplitude perturbation. In Eq. (2), A, B, and D are experimental constants, which are essentially determined by the total number of counts registered, the ratio of scattered light to reference light, and the coherence properties of the optical system. From the correlation time, τ_{C_t}, which is equivalent to the mean life time of the temperature fluctuations observed, the thermal diffusivity a can be calculated by

$$a = \frac{1}{\tau_{C_t}} q^2, \tag{3}$$

where the modulus of the scattering vector q is determined, in addition to the laser wavelength in vacuo, by the scattering geometry of the experiment; see, e.g., Ref. 5.

For SES36, the treatment of the signals resulting from concentration fluctuations as low-amplitude perturbations can be justified, since the diffusion processes are, in general, at least one order of magnitude slower

than the equalization process of thermal fluctuations. Furthermore, for relative differences of the refractive indices of the mixture components of less than 5%, as can be assumed for SES36, the scattered light intensities from temperature fluctuations are in general larger than those from concentration fluctuations [7,8]. It is obvious that the simplified function, Eq. (2), for the determination of the decay time τ_{C_t} is associated with a higher degree of uncertainty than in the case of a pure fluid or a fluid mixture if the refractive indices of the components match, because a larger number of parameters have to be fitted. Depending on the strength of the signals resulting from concentration fluctuations, the total uncertainty for a single measurement is of the order $\pm 1\%$ to $\pm 3\%$.

For the measurement of the sound speed, u_S, the periodic pressure fluctuations, which can be understood as sound waves, are probed. In practice, the frequency ω_S of the sound waves is determined by adding a reference beam, which is shifted relative to the frequency ω_0 of the laser light by $\Delta\omega_M$, by applying an acousto-optical modulator. The frequency shift $\Delta\omega_M$ is of the same order of magnitude as the frequency of the sound waves ($\Delta\omega_M \approx \omega_S$). In this case, the correlation function takes the form:

$$G^{(2)}(\tau) = A + B \exp(-\tau/\tau_C) \cos(\Delta\omega\tau), \tag{4}$$

and the sound speed u_S can be found from a knowledge of the adjusted modulator frequency $\Delta\omega_M$ and the residual detuning $\Delta\omega$, according to

$$u_S = \frac{\omega_S}{q} = \frac{\Delta\omega_M \pm \Delta\omega}{q}. \tag{5}$$

The optical and electro-optical parts of the experimental setup used here for the determination of the thermal diffusivity and sound speed are the same as those employed in our former investigations for toluene and are described in more detail in Refs. 9 and 10. With the exception of the investigation of SES36 in its superheated-vapor phase, the measuring cell system shown in Fig. 2 is identical to that used in our former work with toluene. The sample was kept inside a cylindrical thermostatted pressure vessel (inner diameter, 18 mm; volume $\approx 10\,\text{cm}^3$) made of stainless steel (Hastelloy) and equipped with two quartz windows (Herasil I; diameter, 30 mm; thickness, 30 mm). The temperature in the sample cell, which was placed in an insulated housing, was regulated through resistance heating with a long-term stability better than ± 2 mK. The vessel temperature was measured with a calibrated 25 Ω platinum resistance probe, integrated into the main body of the measuring cell, with a resolution of 0.1 mK using an

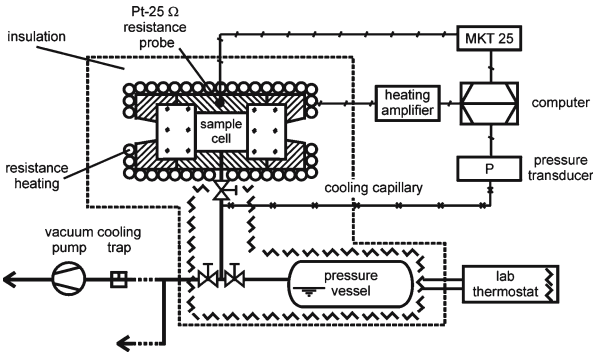

Fig. 2. Measuring cell system with pressure and temperature control for light scattering from bulk fluids.

ac bridge (MKT 25, Anton Paar). The uncertainty of the absolute temperature measurement was less than ±5 mK. For all investigations at saturation conditions, as well as for the measurement of the sound speed in the superheated-vapor phase, typically between four and six single measurements at different values for the modulus of the scattering vector q were performed for each temperature and/or pressure point.

For the investigation of SES36 in its superheated-vapor phase, it was necessary to connect the measuring cell with a pressure vessel (volume $\approx 1\,\mathrm{dm}^3$) through a valve; see Fig. 2. In the pressure vessel, which was thermostatted separately from the measuring cell with the help of a lab thermostat, SES36 was kept in the two-phase region. Thus, the pressure inside the measuring cell corresponded to the adjusted vapor pressure inside the pressure vessel. During a single experimental run, the stability of the pressure in the sample cell was better than ±0.2 kPa. For the measurement of the pressure, the digital pressure reference (RPM1, Desgranges & Huot) was used again (see Sections 2.1 and 2.2), whose absolute measurement uncertainty was less than ±1.5 kPa. The pressure transducer was attached to the measuring cell via a cooling capillary. For the investigation of the thermal diffusivity and speed of sound under saturation conditions, however, the complete filling system, the thermostatted pressure vessel, and the pressure transducer were disconnected from the measuring cell.

2.4. Viscosity and Surface Tension from Surface Light Scattering

In the following, the underlying theory of light scattering by surface waves (surface light scattering, SLS) is briefly reviewed. For a more

detailed and comprehensive description, the reader is referred once again to the specialized literature [11,12]. SLS is a technique, which is closely related to DLS in its classical form; see Section 2.3. The difference is that this technique probes, as the name indicates, fluctuations on the surface of a liquid or, in a more general formulation, at phase boundaries. Liquid–vapor interfaces in macroscopic thermal equilibrium exhibit surface waves, which are caused by thermal movement of molecules and which are quantized in so-called "ripplons." For small viscosities, as is relevant in the experiments described here, the amplitude of surface waves decays in the form of a damped oscillation. SLS analyzes the light scattered by these surface waves.

Here, once again, the experiments are based on a heterodyne detection scheme and signal analysis by PCS. The correlation function of light scattered by surface fluctuations can be described by

$$G^{(2)}(\tau) = A + B\,\cos(\omega_{\mathrm{R}}\tau)\exp(-\tau/\tau_{\mathrm{C_R}}), \tag{6}$$

where the correlation time, $\tau_{\mathrm{C_R}}$, and the frequency, ω_{R}, are identical to the decay time and the frequency of the surface oscillations observed, respectively. As a first-order approximation, the ratio of the sum of the dynamic viscosities of the liquid phase η' and vapor phase η'' to the sum of the densities of the liquid phase ρ' and vapor phase ρ'' may be obtained from the decay time $\tau_{\mathrm{C_R}}$ by

$$\frac{\eta' + \eta''}{\rho' + \rho''} \approx \frac{1}{2\tau_{\mathrm{C_R}} q^2}. \tag{7}$$

Furthermore, the correlation function, Eq. (6), can be simultaneously evaluated for the ratio of the surface tension σ to the sum of the densities of the vapor and liquid phases,

$$\frac{\sigma}{\rho' + \rho''} \approx \frac{\omega_{\mathrm{R}}^2}{q^3}, \tag{8}$$

which to a first-order approximation directly follows from the beat frequency ω_{R} and the wave vector q.

For a reliable determination of viscosity and surface tension, a more detailed and rigorous consideration of the surface light scattering method than that given by Eqs. (6–8) has to be applied. In the present work, therefore, data for the liquid kinematic viscosity and surface tension of SES36 were obtained by an exact numerical solution of the dispersion equation for surface waves at the liquid–vapor interface, see, e.g., Refs. 12 and 13. In addition to the information about the dynamics of the surface fluctuations obtained from the SLS experiment, e.g., frequency ω_{R}, damping Γ

($= 1/\tau_{C_R}$), and the modulus of the wave vector q, reference data for the density of both phases and the dynamic viscosity of the vapor phase under saturation conditions were utilized for this purpose.

In the following, only the sample preparation procedure and experimental conditions are described for the SLS measurements performed on the vapor–liquid interface of SES36. For a detailed description of our SLS apparatus, the reader is referred to Refs. 12 and 14. SES36 was filled from the liquid phase into an evacuated cylindrical pressure vessel (inner diameter, 70 mm; volume, 150 cm^3) made of aluminum and equipped with two quartz windows (Herasil I; diameter, 30 mm; thickness, 30 mm). The temperature regulation of the cell, surrounded by an insulated housing, was realized with electrical heating. For temperatures below room temperature, the insulated housing was cooled to about 10 K below the desired temperature in the sample cell using a lab thermostat. The temperature of the cell was measured with two calibrated 100 Ω platinum resistance probes, integrated into the main body of the vessel, with a resolution of 0.25 mK, using an ac bridge (MKT 100, Anton Paar). The uncertainty of the absolute temperature measurement was less than ±15 mK. The temperature stability during an experimental run was better than ±2 mK. For each temperature, at least six measurements at different values of the modulus of the scattering vector were performed.

3. RESULTS AND DISCUSSION

In the following section, experimental results for the vapor pressure, density, thermal diffusivity, sound speed, viscosity, and surface tension of the azeotropic refrigerant mixture SES36 are presented and discussed. Due to the fact that neither equilibrium data nor transport properties of SES36 can be found in the literature, a data comparison could be drawn for this first published data set only with theoretically calculated or predicted data. In general, regarding the properties of pure R365mfc, see, e.g., Refs. 15 and 16, at a given temperature, the mixture results for density, vapor pressure, and viscosity exhibit higher values, while for sound speed, surface tension, and thermal diffusivity, lower values can be found.

3.1. Vapor Pressure

The experimental values for the vapor pressure of SES36 are listed in Table I and are depicted, along with the distribution of our p, ρ, T data, in the upper part of Fig. 3. In the lower part of Fig. 3, the deviations of the experimental results for the vapor pressure from their correlation given by Eq. (9) are shown. The experimental values for the vapor pressure p_S

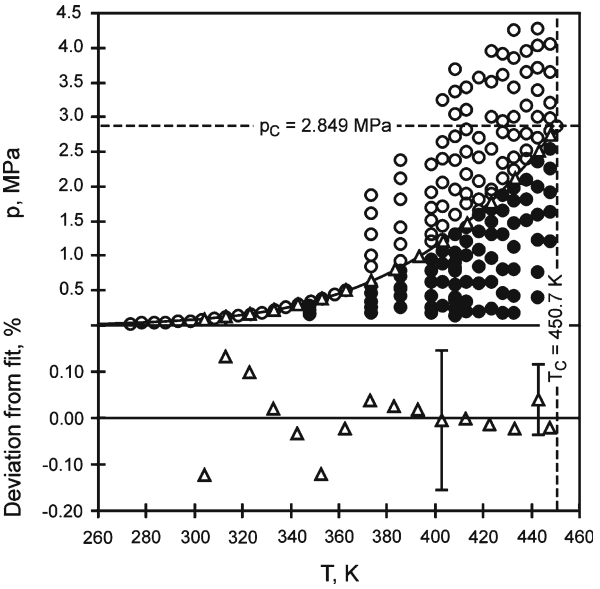

Fig. 3. Vapor pressure p_S and distribution of the p, ρ, T data for SES36 (△, vapor-pressure data; —, saturation line, Eq. (9); ◘, critical point; ○, liquid-phase p, ρ, T data; •, vapor-phase p, ρ, T data).

can be well represented within the experimental uncertainty of ±2 kPa by a Wagner-type equation [17],

$$\ln(p_S/\text{MPa}) = A_1 + (A_2\varepsilon + A_3\varepsilon^{1.5} + A_4\varepsilon^{2.5} + A_5\varepsilon^5)/T_R, \tag{9}$$

where T is the absolute temperature, $\varepsilon = 1 - T_R$, $T_R = T/T_C$ is the reduced temperature, and T_C is the critical temperature. The latter was determined in this work to be 450.7 ± 0.5 K and was derived from experimental values of the thermal diffusivity; see Section 3.3. The fit parameters of Eq. (9), which represents the experimental data for the vapor pressure with a root-mean-square deviation of 0.064% or 0.35 kPa, are $A_1 = 1.047091$, $A_2 = -7.888361$, $A_3 = 2.272983$, $A_4 = -4.504416$, and $A_5 = 14.732086$. The critical pressure $p_C = 2.849$ MPa ± 0.024 MPa was determined by extrapolating Eq. (9) to the critical temperature. Using Eq. (9) and the derived critical pressure p_C, the acentric factor $\omega = -1 - \log p_R|_{T_R = 0.7}$ of SES36 was calculated to be 0.352 ± 0.008 according to Pitzer [18, 19]. Here, $p_R = p_S/p_C$ is the reduced saturated-vapor pressure.

Table I. Experimental Values of the Vapor Pressure p_S of SES36

T (K)	p_S (MPa)	T (K)	p_S (MPa)
304.15	0.086	383.15	0.792
313.15	0.117	393.15	0.982
323.15	0.162	403.15	1.204
333.15	0.220	413.15	1.462
343.15	0.293	423.15	1.760
353.15	0.384	433.15	2.104
363.15	0.496	443.15	2.504
373.15	0.631	448.15	2.726

3.2. Density

3.2.1. Superheated-Vapor Density

The p, ρ, T measurements in the superheated-vapor region along 14 isotherms over the temperature range between 347 and 448 K and pressure range between 0.1 and 2.5 MPa are summarized in Table II. First, for analyzing the experimental data and for extrapolating these to saturation conditions, each isotherm was fitted by a virial equation of state of the form,

$$p = \frac{RT}{Mv}\left(1 + \frac{B}{v} + \frac{C}{v^2}\right), \tag{10}$$

where $R = 8.31441\ \mathrm{J \cdot mol^{-1} \cdot K^{-1}}$ is the universal gas constant, T is the absolute temperature in K, $M = 0.18485\ \mathrm{kg \cdot mol^{-1}}$ is the molar mass of SES36, $v(=1/\rho)$ is the specific volume in $\mathrm{m^3 \cdot kg^{-1}}$, and B and C are the second and third virial coefficients, respectively. Due to the relatively large experimental uncertainty in the gas-phase density of ±0.3% at 2.5 MPa to ±3% at 0.1 MPa, a second fit parameter did not significantly improve the data representation, especially at low temperatures. Thus, by fitting B and C, for all isotherms the experimental data for the pressure are represented with an absolute average deviation of 0.55% which is close to the value of 0.57% obtained when truncating Eq. (10) after the second term for reduced temperatures $T_R < 0.93$. For the latter case, Fig. 4 shows the results of the first data analysis in the form of deviations of the experimental data for the gas-phase density from those calculated by Eq. (10) using the individual fit parameters, where an absolute average deviation of 0.7% can be found. The dashed curves represent the estimation of the overall uncertainty of the density, as described in Section 2.2.

In contrast to light gases, third virial coefficients of polar refrigerants contribute significantly to the density, and they must be taken into

Table II. Experimental Values of the Vapor Density of SES36 along 14 Isotherms at Temperatures between 347 and 448 K

p (MPa)	ρ (kg·m^{-3})	p (MPa)	ρ (kg·m^{-3})	p (MPa)	ρ (kg·m^{-3})	p (MPa)	ρ (kg·m^{-3})
$T = 347.83$ K		$T = 403.07$ K		$T = 418.19$ K		$T = 432.89$ K	
0.153	10.6	0.275	16.0	0.600	35.4	1.479	101.4
0.191	13.5	0.627	39.6	0.845	52.8	1.799	141.0
0.226	15.5	0.891	59.6	1.086	71.7	1.980	172.4
0.281	20.3	1.071	77.7	1.354	98.9	$T = 437.93$ K	
$T = 373.25$ K		$T = 408.13$ K		1.594	134.3	1.508	101.3
0.190	11.4	0.141	7.8	$T = 423.09$ K		1.813	135.2
0.253	16.2	0.246	13.9	0.241	13.3	2.091	178.6
0.334	21.7	0.357	20.7	0.622	36.9	$T = 442.74$ K	
0.465	32.2	0.407	23.9	0.972	61.7	0.399	21.1
0.558	38.9	0.593	36.2	1.309	91.9	0.760	42.5
$T = 385.41$ K		0.780	49.9	1.486	112.4	1.235	76.2
0.270	16.3	0.818	52.9	1.673	138.4	1.593	107.5
0.422	27.1	0.899	60.2	$T = 428.03$ K		1.988	152.1
0.529	34.5	1.059	73.5	0.181	9.6	2.355	223.8
0.554	36.8	1.315	105.5	0.461	25.5	$T = 447.81$ K	
0.701	48.3	$T = 413.17$ K		0.810	48.4	1.208	72.8
0.779	55.7	0.196	10.9	1.310	87.6	1.637	108.2
$T = 398.44$ K		0.347	20.2	1.648	125.4	1.916	135.5
0.177	10.1	0.634	39.2	1.883	166.6	2.251	182.3
0.256	15.0	1.009	67.2	$T = 432.89$ K		2.548	251.1
0.420	26.2	1.211	88.2	0.173	9.3		
0.629	40.6	1.408	114.6	0.432	23.7		
0.781	54.1	$T = 418.19$ K		0.800	47.3		
0.951	69.0	0.208	11.4	1.128	71.0		

account even at moderate pressures. Furthermore, at the density of the saturated vapor, the third virial coefficient should be included down to a reduced temperature of about 0.75 [20]. For a convincing data representation over the complete temperature range investigated in this work, as well as for an improvement of the extrapolation of the vapor-phase data to saturation conditions, a second data analysis was performed by adopting in Eq. (10) the third virial coefficient from the empirical prediction method of Liu and Xiang [21], which is based on a simple extended corresponding-states principle. The method is capable of predicting properties of polar fluids and describing the third virial coefficient as an universal function of the reduced temperature in terms of substance parameters, e.g., the critical compressibility factor $Z_C = p_C M/(R\rho_C T_C)$ and the acentric factor ω. On the basis of $Z_C = 0.261$, resulting from the already mentioned critical parameters $p_C = 2.849$ MPa and $T_C = 450.7$ K, the critical density $\rho_C =$

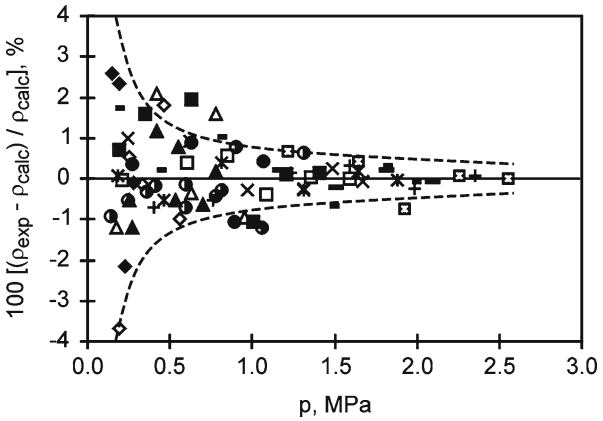

Fig. 4. Deviations of the experimental data ρ_{exp} for the vapor density of SES36 from the calculated values ρ_{calc} of the virial equation of state, Eq. (10), for 14 isotherms at temperatures between 347 and 448 K (♦, 347.83 K; ◇, 373.25 K; ▲, 385.41 K; △, 398.44 K; •, 403.07 K; ◑, 408.13 K; ■, 413.17 K; □, 418.19 K; ×, 423.09 K; ✱, 428.03 K; ▬, 432.89 K; ▬, 437.93 K; +, 442.74 K; ⊡, 447.81 K) as a function of pressure.

538 $kg \cdot m^{-3}$ determined also within this work, and $\omega = 0.352$, for the third virial coefficient C of SES36, the prediction method of Liu and Xiang [21] results in

$$C(T_R)\rho_C^2 = 0.9594 \times 10^{-3} + 0.8746286 T_R^{-3} - 0.1575841 T_R^{-6} - 0.0448993 T_R^{-11}. \quad (11)$$

The second and third virial coefficients of SES36 as a function of the reduced temperature are shown in Fig. 5. The open symbols represent the coefficients resulting from the first analysis of our experimental p, ρ, T-data when truncating Eq. (10) after the second term for $T_R < 0.93$, where the exemplarily depicted error bars represent 99% confidence limits for the fitted parameters. The strongly increasing uncertainty in the third virial coefficient with decreasing temperature confirms that at low temperature the fit is not sensitive to a second fit parameter. The closed symbols in Fig. 5 represent the second virial coefficients based on the second analysis of our experimental p, ρ, T data according to Eq. (10), where now the third virial coefficients have been calculated by Eq. (11). The predicted data for the third virial coefficient are represented by the dotted line in Fig. 5. The second virial coefficients obtained by means of the predicted third virial coefficients and from our experimental p, ρ, T data can well be

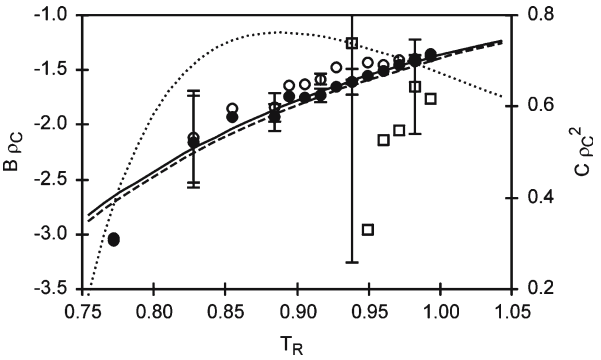

Fig. 5. Second and third virial coefficients B and C, respectively, of SES36 as a function of the reduced temperature (B: ○, this work – truncating Eq. (10) after the second term for $T_R < 0.93$; •, this work – adopting C in Eq. (10) from corresponding-states principle, Eq. (11) [21]; —, this work, Eq. (12); – – –, corresponding-states principle [22]/C: □, this work; ⋯, corresponding-states principle, Eq. (11) [21]).

represented by a simple empirical equation with three adjustable parameters,

$$B(T_R)\rho_C = 4.85431 T_R^{-3/4} \exp(-0.3366449 T_R^{-3}) - 4.82851 T_R^{-1/2}, \quad (12)$$

which is indicated by the solid line in Fig. 5. This type of correlation was found to be suitable for a representation of the temperature behavior of the second virial coefficient for halocarbon substances by Xiang [22]. For the evaluation of Eq. (12), we have taken into account different uncertainties for the second virial coefficients by an adequate weighting procedure. By combining Eq. (10) with Eqs. (11) and (12), as applied for the extrapolation of the present vapor-phase data to saturation conditions, however, the experimental data for the pressure can be represented with an absolute average deviation of 0.83% over the complete temperature range investigated. For the experimental density data, a corresponding value of 1.06% can be found. For comparison purposes, predicted data for the second virial coefficient, based again on a simple extended corresponding-states principle as given by Xiang [22], are also included as a dashed line in Fig. 5. Using the methods of Xiang [22] and Liu and Xiang [21] for calculation of the second and third virial coefficients, respectively, an absolute average deviation of 1.3% can be found between the experimental and calculated data for the pressure.

3.2.2. Compressed-Liquid Density

The major aim of the measurements in the compressed-liquid phase was to extend the information about the saturated-liquid density of SES36 at elevated temperatures. Here, measurements were performed along 13 isotherms ranging between 373 and 448 K at pressures starting close to the saturation line and up to a maximum of about 4 MPa. The experimental data for the compressed-liquid density are summarized in Table III and Fig. 6. Here, the symbols represent the experimental data and the solid lines their empirical correlations. While for reduced temperatures $T_R < 0.95$, the experimental data could be represented within the estimated uncertainty of $\pm 0.3\%$ by a linear equation, for $T_R > 0.95$ a three-parameter fit in the form of a potential function was used. The absolute average deviation of the experimental density data for the compressed-liquid phase from those calculated with the individual fits for each isotherm is smaller than 0.1%. In addition, in Fig. 6 saturated-liquid-density values are shown, which could be obtained by extrapolation of the respective data correlation for each isotherm.

3.2.3. Saturated Densities

The values for the liquid and vapor densities of SES36 under saturation conditions obtained for temperatures between 347 and 448 K by extrapolating the corresponding data sets for the compressed-liquid and superheated-vapor phases to the saturation pressure, respectively, are listed in Table IV. Although for both phases, measurements were also performed close to the saturation line, the uncertainty introduced by the extrapolation procedure dominates the total uncertainty of about $\pm 1 - \pm 2\%$ and $\pm 2 - \pm 5\%$ for the saturated-liquid and -vapor densities, respectively. The uncertainty could be estimated from fits to different fit intervals by varying the density values included in the fit. The experimental results obtained with the density meter DMA 5000 for the density of the liquid phase of SES36 under true saturation conditions are summarized in Table V. Here, the listed data are average values of two independent measurement series with new samples within the U-tube of the density meter. These measurements agreed within $\pm 0.05\%$. The total uncertainty of the density measurements under true saturation conditions is estimated to be less than $\pm 0.1\%$.

On the basis of a corresponding-states correlation of saturated-liquid volumes, we have predicted the saturated-liquid density over a range of reduced temperatures of 0.56–1.00 by $\rho = 1/[v_{SC} v_R^{(0)}(1 - \omega\delta)]$ [23], where the generalized functions $v_R^{(0)}$ and δ are dependent only upon the

Table III. Experimental Values of the Liquid Density of SES36 along 13 Isotherms at Temperatures between 373 and 448 K

p (MPa)	ρ (kg·m^{-3})	p (MPa)	ρ (kg·m^{-3})	p (MPa)	ρ (kg·m^{-3})	p (MPa)	ρ (kg·m^{-3})
$T = 373.24$ K		$T = 403.07$ K		$T = 418.20$ K		$T = 437.92$ K	
0.838	1,156.7	2.392	1,058.0	2.711	991.7	2.406	860.9
1.003	1,158.9	2.635	1,062.9	3.572	1,011.4	2.513	868.1
1.302	1,162.3	3.244	1,074.3	$T = 423.11$ K		2.772	881.0
1.606	1,164.4	$T = 408.11$ K		1.895	955.8	3.176	896.0
1.875	1,164.6	1.447	1,020.3	1.949	956.9	3.662	911.5
$T = 385.41$ K		1.651	1,022.3	2.550	968.1	3.951	920.7
0.927	1,108.8	1.886	1,024.5	2.999	976.5	$T = 442.76$ K	
1.165	1,113.6	2.087	1,027.3	3.506	988.6	2.704	808.5
1.410	1,117.6	2.406	1,032.9	3.952	1,000.1	3.004	838.3
1.826	1,124.3	2.819	1,041.5	$T = 428.04$ K		3.389	862.7
2.123	1,128.3	3.632	1,057.6	2.125	932.5	3.706	877.2
2.381	1,130.9	$T = 413.15$ K		2.347	936.5	4.027	890.2
$T = 398.42$ K		1.749	1,004.2	2.784	943.7	4.278	899.9
1.206	1,061.5	1.893	1,006.2	2.940	946.8	$T = 447.83$ K	
1.319	1,062.9	2.184	1,009.3	3.604	962.5	2.797	715.2
1.511	1,065.4	2.500	1,014.5	3.905	970.8	2.987	763.1
1.698	1,068.0	2.815	1,020.8	$T = 432.89$ K		3.217	798.3
1.913	1,071.5	3.115	1,027.4	2.236	901.2	3.653	840.9
2.313	1,079.0	3.431	1,034.6	2.420	907.9	4.056	863.9
$T = 403.07$ K		$T = 418.20$ K		2.745	917.7		
1.222	1,037.5	1.660	978.0	3.002	923.8		
1.429	1,041.1	1.824	979.7	3.432	934.8		
1.721	1,046.3	2.077	982.5	3.852	946.7		
2.067	1,051.8	2.428	986.8	4.256	958.6		

reduced temperature. Here, the scaling volume $v_{SC} = v_{ref}/[v_{R,ref}^{(0)}(1 - \omega\delta_{ref})]$ is expressed by the quantities $v_{R,ref}^{(0)}$ and δ_{ref}, which denote the evaluation of the generalized functions at the reference temperature, for which the density $\rho_{ref}(= 1/v_{ref})$ is known. On the basis of the acentric factor $\omega = 0.352$ and using the saturated-liquid density at a temperature of 363.15 K as a reference point, e.g., $\rho_{ref} = 1,186.8\,\mathrm{kg \cdot m^{-3}}$, by the extrapolation of the prediction method to the critical temperature ($T_R \to 1$) the critical density ρ_C of SES36 was estimated to be $538\,\mathrm{kg \cdot m^{-3}}$.

For both phases, the saturated densities were correlated by

$$\rho = \rho_C \left(1 + \sum_{i=1}^{5} \rho_i \varepsilon^{i/3} \right), \tag{13}$$

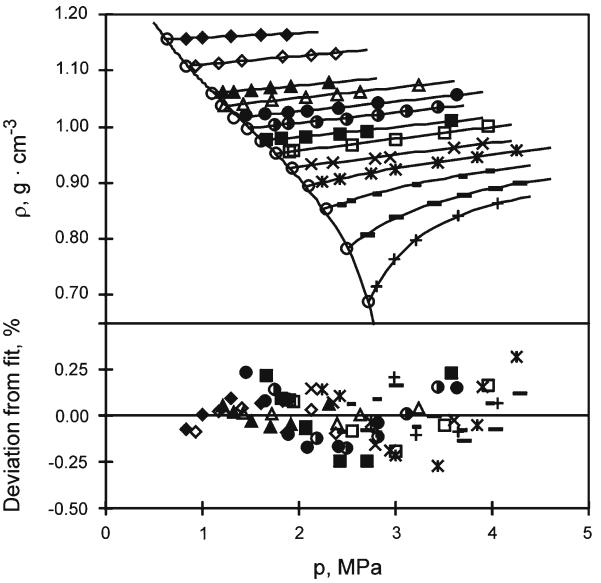

Fig. 6. Liquid density ρ of SES36 along 13 isotherms at temperatures between 373 and 448 K (♦, 373.24 K; ◇, 385.41 K; ▲, 398.42 K; △, 403.07 K; •, 408.11 K; ◑, 413.15 K; ■, 418.20 K; □, 423.11 K; ×, 428.05 K; ✱, 432.89 K; ▬, 437.92 K; ▬, 442.76 K; +, 447.83 K) and at saturation conditions (○) as a function of pressure.

Table IV. Data for the Liquid and Vapor Densities of SES36 under Saturation Conditions

Liquid phase		Vapor phase	
T (K)	ρ' (kg · m^{-3})	T (K)	ρ'' (kg · m^{-3})
373.24	1,156.0	347.83	24.2
385.41	1,108.3	373.25	46.2
398.42	1,059.2	385.41	61.9
403.07	1,036.8	398.44	84.0
408.11	1,015.8	403.07	93.6
413.15	997.6	408.13	105.4
418.20	975.0	413.17	118.9
423.11	952.2	418.19	134.3
428.04	926.8	423.09	151.9
432.89	894.1	428.03	172.9
437.92	854.5	432.89	198.2
442.76	782.3	437.93	231.7
447.83	688.8	442.74	274.5
		447.81	331.3

Table V. Experimental Values of the Liquid Density of SES36 under Saturation Conditions

T (K)	ρ' (kg · m^{-3})	T (K)	ρ' (kg · m^{-3})
273.14	1,422.3	323.15	1,302.2
278.15	1,410.9	328.15	1,288.6
283.15	1,399.6	333.15	1,274.8
288.15	1,388.7	338.15	1,260.7
293.15	1,377.5	343.15	1,246.8
298.15	1,365.9	348.15	1,232.3
303.15	1,353.6	353.15	1,217.6
308.15	1,341.1	358.15	1,202.5
313.15	1,328.4	363.15	1,186.8
318.15	1,315.4		

Table VI. Coefficients of Eq. (13)

ρ_i	Saturated density	
	Liquid phase	Vapor phase
ρ_1	−0.3968	−3.5243
ρ_2	17.9889	15.0458
ρ_3	−52.375	−51.382
ρ_4	67.9231	77.8232
ρ_5	−31.7301	−41.6172
T-range (K)	273–448	348–448
rms (%)	0.38	0.87

where the coefficients are given in Table VI. While for the vapor phase, only extrapolated data from the p, ρ, T measurements enter into the correlation; for the liquid phase, the measurements under true saturation conditions were additionally taken into account. For correlation of the complete set of data for the saturated-liquid phase, the statistical weight of each data point has been assumed to be the inverse of its estimated uncertainty.

In Fig. 7, the liquid and vapor densities of SES36 under saturation conditions have been plotted in the upper part in comparison with prediction methods. Here, also the midpoints of the coexistence curve $(\rho' + \rho'')/2$ are shown. Their temperature dependence should follow the classical law of the rectilinear diameter. By extrapolation of $(\rho' + \rho'')/2$ from 445 K to the critical temperature, the critical density is determined to be 2.4% lower than the predicted value. In the lower part of Fig. 7, the

deviations between the correlations, Eq. (13), developed from our results and the prediction methods are shown. Included in Fig. 7 are predicted values for the saturated-liquid density based on a corresponding-states correlation [23], as already mentioned above. The prediction matches our experimental value at 363.15 K, because it was used as a reference point. The variability of the prediction close to this point is due to its diverse formulation for reduced temperatures, $0.20 < T_R < 0.80$ and $0.80 < T_R < 1.0$ [23]. The prediction has been verified for different substances, where in comparison to experimental data maximum deviations of less than 2.2% for all compounds, except for highly polar ones, are determined. Below a reduced temperature of 0.8, maximum deviations are almost always less than 0.5%. For the complete temperature range studied in this work, an absolute average deviation of 0.53% can be found between our density data and predicted results, whereby a maximum deviation of 2.49% is obtained for the data point at a temperature of 437.92 K. Excluding the temperature range $T_R > 0.80$, the corresponding deviation is reduced to 0.18%. Finally, saturated-vapor densities calculated by the Chen equation [24,25] have been included in Fig. 7. This equation represents an universal p, v, T equation for gases at saturation based on the corresponding-states principle and has been checked by different working fluids including polar substances, for which, in comparison with data recommended in the literature, an absolute average deviation of 0.43% is reported [24,25]. The absolute average deviation of the data of this work from the Chen equation [24,25] is 0.88%. This value is only 0.13% larger than the value obtained in comparing our data with their correlation, Eq. (13).

3.3. Thermal Diffusivity and Sound Speed

The experimental data for thermal diffusivity and sound speed of SES36 in the saturated-liquid and -vapor phases obtained by light scattering from bulk fluids are plotted in Figs. 8 and 9, respectively, and are summarized in Table VII. In the figures, the open and closed symbols represent the mean value of up to six single measurements at different angles of incidence and distinguish between the liquid and vapor phases, respectively. The exemplarily depicted error bars for the thermal diffusivity and sound speed of SES36 in the saturated-liquid phase represent the total uncertainties, which could be estimated to be less than ±2% and ±0.5%, respectively, except for a few data points close to the critical point. The evaluation of the uncertainties is based on the standard deviation of single measurements, which may be regarded as a direct measure of the uncertainty of data by DLS from bulk fluids [26]. The larger uncertainty of the results for the thermal diffusivity of SES36 in comparison to former

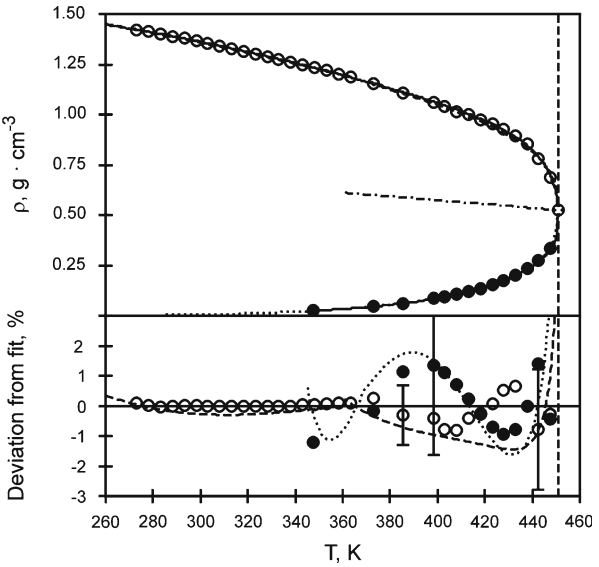

Fig. 7. Liquid and vapor density ρ' and ρ'', respectively, of SES36 under saturation conditions as a function of temperature (○, liquid phase; ●, vapor phase; – – –, prediction method $\rho' = f(T_R, \omega, \rho_{ref})$ [23]; ···, Chen equation $\rho'' = f(T_R, p_R, \rho_C)$ [24, 25]; – · –, midpoints $(\rho' + \rho'')/2$; ◘, critical point).

investigations by DLS for pure fluids and fluid mixtures with small differences of refractive indices of its components can be attributed to a superposition of signals observable from both thermal and mass diffusion; see Section 2.3. Approaching the critical point of SES36, an increasing standard deviation for the thermal diffusivity and sound-speed measurements of ±3% and ±1%, respectively, could be observed. This behavior can be attributed to an increasing experimental complexity in the critical region. The solid lines in Figs. 8 and 9 are empirical correlations of our experimental data. The thermal diffusivity, as well as the sound speed, for both liquid and vapor phases, can be well represented within the experimental uncertainty by a sum of a polynomial and an additional term, which takes into account the curvature to the critical point, resulting in an equation of the form,

$$y = \sum_{i=0}^{2} y_i (T/\mathrm{K})^i + \frac{y_3}{(T - T_C^*)/\mathrm{K}}, \tag{14}$$

Table VII. Experimental Values of the Thermal Diffusivity a and Sound Speed u_S of SES36 under Saturation Conditions

Thermal diffusivity				Sound speed			
Liquid phase		Vapor phase		Liquid phase		Vapor phase	
T (K)	a (10^{-8} m^2·s^{-1})	T (K)	a (10^{-8} $m^2 \cdot s^{-1}$)	T (K)	u_S (m·s^{-1})	T (K)	u_S (m·s^{-1})
298.15	3.92	418.15	11.08	293.20	650.9	373.15	111.2
323.15	3.57	420.65	10.24	313.19	585.4	383.15	108.1
348.15	3.21	423.15	9.59	333.16	514.4	393.15	104.6
353.15	3.19	425.65	8.78	353.12	445.2	398.15	102.4
373.15	2.99	428.15	7.99	363.10	408.8	403.15	100.1
383.15	2.84	430.65	7.33	363.19	410.9	408.15	97.34
393.15	2.77	433.15	6.55	373.00	373.9	413.15	94.48
403.15	2.69	435.65	5.75	383.15	337.3	415.65	92.93
413.15	2.54	438.15	4.92	393.15	300.6	418.15	90.94
423.15	2.45	440.65	4.04	403.15	264.6	420.65	89.58
433.15	2.28	443.15	3.14	413.15	226.5	423.15	87.71
438.15	2.09	445.65	2.22	423.15	186.7	425.65	85.69
440.65	1.96	447.15	1.56	433.15	143.6	428.15	83.47
443.15	1.74	448.15	1.17	438.15	120.1	430.65	81.27
444.15	1.65	449.15	0.751	440.65	107.8	433.15	79.01
445.15	1.49			443.15	95.11	435.65	76.48
446.15	1.32			444.15	89.58	438.15	73.77
447.15	1.14			445.15	84.50	440.65	71.13
				447.15	72.47	443.15	67.96
				448.15	66.67	445.65	64.77
						447.15	62.45
						448.15	61.04
						449.15	59.47

where the coefficients y_i and the additional fit parameter T_C^* are given in Table VIII. Here, also the root-mean-square deviations of our values from Eq. (14) and the ranges of validity are stated. For both phases, the root-mean-square deviations of our sound-speed data from Eq. (14) is clearly less than 0.5%. Somewhat worse is the situation for the thermal-diffusivity data, where a root-mean-square deviation of about 0.9% can be found for both phases.

The critical temperature of SES36 could be determined by extrapolating the experimental values for thermal diffusivity obtained at reduced temperatures larger than 0.9 to zero, which is true at the critical point. By applying this procedure to the vapor and liquid phases followed by averaging of these results, which exhibit a difference of about 0.2 K, a critical temperature of 450.7 ± 0.5 K was determined for SES36.

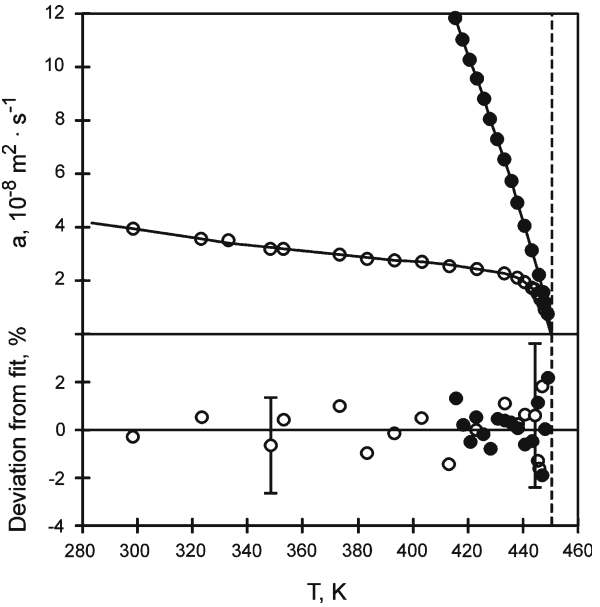

Fig. 8. Thermal diffusivity a of SES36 under saturation conditions as a function of temperature (○, liquid phase; ●, vapor phase).

Table VIII. Coefficients of Eq. (14)

y_i	Thermal diffusivity a, y_i ($10^{-8}\,m^2 \cdot s^{-1}$)		Sound speed u_S, y_i ($m \cdot s^{-1}$)	
	Liquid phase	Vapor phase	Liquid phase	Vapor phase
y_0	13.1462	1529.4766	1590.04	−187.465
y_1	−0.045496	−7.282341	−2.99786	1.80529
y_2	4.9675×10^{-5}	1.001485×10^{-2}	-0.6076×10^{-3}	-2.598×10^{-3}
y_3	10.118	35,957.3	1,228.1	1,521.5
T_C^* (K)	453.40	578.386	469.28	487.41
T-range (K)	298–447	418–449	293–448	373–449
rms (%)	0.91	0.89	0.24	0.11

It is worth mentioning that the azeotropic characteristic of SES36 could be confirmed by the observed convergent behavior of liquid- and vapor-phase data for the thermal diffusivity, as well as for the sound speed, at the critical point. Both quantities were investigated in order, starting in the saturated-liquid phase up to the vapor–liquid critical point and from there along the dew line, lowering the temperature. For keeping

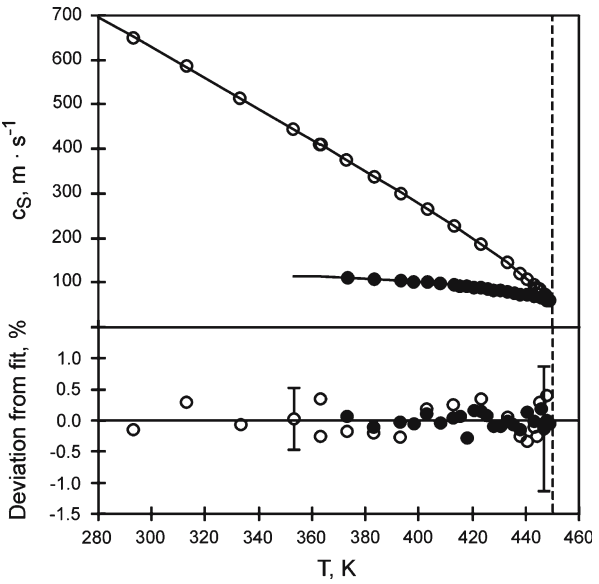

Fig. 9. Sound speed u_S of SES36 under saturation conditions as a function of temperature (○, liquid phase; ●, vapor phase).

the sample at true saturation conditions after and also during a change in temperature, the filling height of the sample in the measuring cell had to be controlled and adjusted newly by evaporating small amounts of the sample. For the case of a non-azeotropic mixture, the above-described process would not show the convergence behavior found for SES36.

In Table IX and Fig. 10, the experimental results for the sound speed in the superheated-vapor phase are summarized. In addition, values for the sound speed for the saturated-vapor phase as already shown in Fig. 9 and for the ideal-gas state ($p \to 0$) are shown in Fig. 10. The last-mentioned values were derived with the help of fundamental thermodynamics, $u_S^2 = T R/M[c_p^0/(c_p^0 - R)]$, from theoretical calculated values of the molar ideal-gas heat capacity at constant pressure c_p^0. For the ideal-gas state the molar heat capacity of a mixture at constant pressure is given by the molar weighted sum of the pure-component data. For this, the molar heat capacity of the pure components of SES36 were calculated by using the group contribution method of Joback [27] as reported in Ref. 28. Over the temperature range from 273 to 613 K, the calculated molar ideal-gas heat capacity at constant pressure of SES36 as a function of temperature can

Table IX. Experimental Values of the Sound Speed u_S of SES36 in the Vapor Phase

p (MPa)	u_S ($m \cdot s^{-1}$)	p (MPa)	u_S ($m \cdot s^{-1}$)	p (MPa)	u_S ($m \cdot s^{-1}$)
$T = 393.15$ K		$T = 433.15$ K		$T = 473.15$ K	
0.621	118.33	1.650	100.79	0.643	139.97
0.733	113.95	1.842	92.96	0.923	135.95
0.826	109.91	1.956	86.80	1.217	131.02
$T = 413.15$ K		$T = 443.15$ K		1.578	123.97
0.622	125.04	0.644	132.81	1.871	118.26
0.712	121.48	0.865	128.34	2.190	111.52
0.913	115.68	1.047	123.29	2.416	106.45
1.101	108.63	1.241	118.91	$T = 498.15$ K	
1.298	101.02	1.448	113.37	0.643	146.41
$T = 423.15$ K		1.649	107.61	0.923	142.50
0.621	127.48	1.841	101.22	1.242	137.57
0.821	123.70	2.040	93.87	1.573	133.76
0.991	117.78	2.248	84.40	1.877	130.63
1.142	111.52	2.376	76.81	2.204	126.37
1.309	105.59	$T = 453.15$ K		2.417	122.69
1.525	96.98	0.621	136.01	$T = 523.15$ K	
$T = 433.15$ K		0.938	130.53	0.926	149.45
0.644	130.36	1.230	124.12	1.227	145.77
0.865	125.43	1.566	115.99	1.541	142.65
1.047	120.76	1.854	108.36	1.883	140.19
1.241	114.90	2.190	97.86	2.201	136.78
1.448	108.37	2.415	89.88	2.419	133.96

be well represented by a polynomial of third order,

$$c_p^0(T)/R = -4.43 + 0.1084(T/\mathrm{K}) - 1.099 \times 10^{-4}(T/\mathrm{K})^2 + 4.256 \times 10^{-8}(T/\mathrm{K})^3. \quad (15)$$

Of course, due to the limitation of the present sound-speed data at pressures above 0.5 MPa and their relatively large uncertainty of ±0.5%, the results of this work cannot be used for evaluating c_p^0 by an adequate extrapolation procedure. On the contrary, the theoretically calculated data for c_p^0 can confirm the applicability of the DLS-technique for measurements of the sound speed in the superheated region, which were carried out, to the best of our knowledge, for the first time within the present work.

The solid lines in Fig. 10 represent an individual data correlation for each isotherm. Values obtained by the extrapolation of the individual fits to the saturation line are in agreement with the measured results. In this way, the azeotropic characteristic of SES36 could be confirmed again,

Table X. Liquid Kinematic Viscosity ν' and Surface Tension σ of SES36 Under Saturation Conditions[a]

T (K)	η'' (μPa·s)	ρ' (kg·m^{-3})	ρ'' (kg·m^{-3})	ν' (mm^2·s^{-1})	σ (mN·m^{-1})
253.15	9.15	1,459.1	0.96	0.7135	16.87
263.15	9.46	1,440.9	1.46	0.6098	16.12
273.15	9.83	1,421.2	2.18	0.5279	15.29
283.15	10.2	1,400.1	3.18	0.4540	14.26
293.15	10.7	1,377.6	4.56	0.3968	13.29
303.15	11.1	1,353.8	6.43	0.3583	12.36
313.15	11.6	1,328.8	8.89	0.3199	11.32
323.15	12.0	1,302.6	12.1	0.2886	10.40
333.15	12.4	1,275.1	16.2	0.2574	9.43
343.15	12.8	1,246.5	21.5	0.2334	8.46
353.15	13.2	1,216.8	28.1	0.2102	7.51
363.15	13.6	1,185.8	36.4	0.1907	6.59
373.15	14.1	1,153.4	46.6	0.1758	5.66
383.15	14.6	1,119.5	59.0	0.1593	4.74
393.15	15.3	1,083.6	74.5	0.1461	3.92
403.15	16.2	1,044.8	93.8	0.1310	3.06
413.15	17.2	1,001.7	118.6	0.1181	2.27

[a] Directly measured values for frequency ω_R and damping Γ at a defined wave vector q of surface waves were combined with theoretically calculated values for ρ'' and η'' according to Refs. 24 and 25 and Refs. 28 and 29, respectively, and our own data for ρ' to derive ν' and σ by an exact numerical solution of the dispersion relation.

since for measurement of the sound speed in the superheated and saturated regions, different setups were used. While for the investigation under saturation conditions a closed measurement cell was used, for the superheated region it was connected with a pressure vessel, where the refrigerant mixture was kept in the two-phase region, see Section 2.3, and demixing would have been possible for a non-azeotropic or near-azeotropic mixture.

3.4. Viscosity and Surface Tension

The results from surface light scattering for the liquid kinematic viscosity and surface tension of SES36 under saturation conditions are summarized in Figs. 11 and 12, respectively, and listed in Table X. The data represent average values of typically six to eight independent measurements at different angles of incidence. Besides the results for the kinematic viscosity and surface tension, Table X includes the reference data used for the data evaluation; see Section 2.4. The density of the saturated-liquid phase ρ' was taken from our own measurements. The density of the

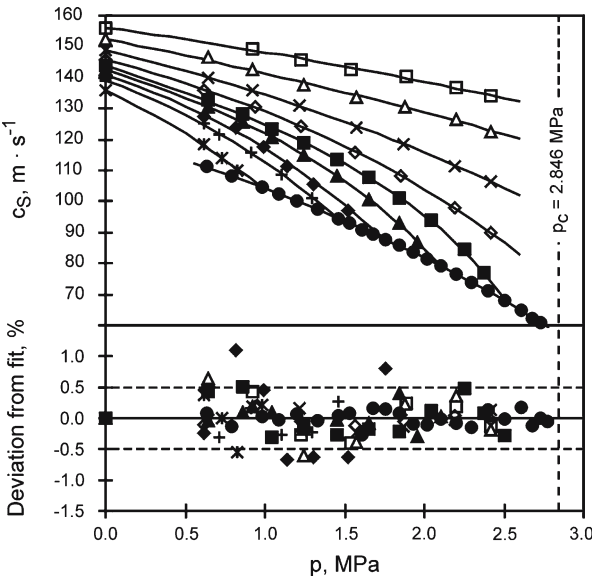

Fig. 10. Sound speed u_S of the vapor phase of SES36 along nine isotherms at temperatures between 393 and 523 K (✱, 393.15 K; +, 413.15 K; ♦, 423.15 K; ▲, 433.15 K; ■, 443.15 K; ◇, 453.15 K; ×, 473.15 K; △, 498.15 K; □, 523.15 K) and at saturation conditions (●) as a function of pressure.

saturated-vapor phase ρ'' was calculated by the Chen equation [24, 25], which is in good agreement with our data set at high temperatures. Furthermore, the dynamic viscosity in the saturated-vapor phase η'' was calculated according to a method given in Refs. 28 and 29. Taking into account the uncertainties of the individual quantities entering the calculation, the uncertainty of our liquid kinematic viscosity data for SES36 is estimated to be less than $\pm 1.5\%$ for the complete temperature range investigated in this work. For the surface tension, the uncertainty is also estimated to be less than $\pm 1.5\%$. It should be noted that even approximate values for the dynamic viscosity of the vapor phase are sufficient to achieve such an accuracy. A more detailed discussion regarding the accuracy achievable for liquid kinematic viscosity and surface tension from SLS can be found in Refs. 12 and 14.

For the complete temperature range studied, a modified Andrade-type equation, which in its simple form is commonly chosen to represent the dynamic viscosity at least over a limited temperature range, was used in

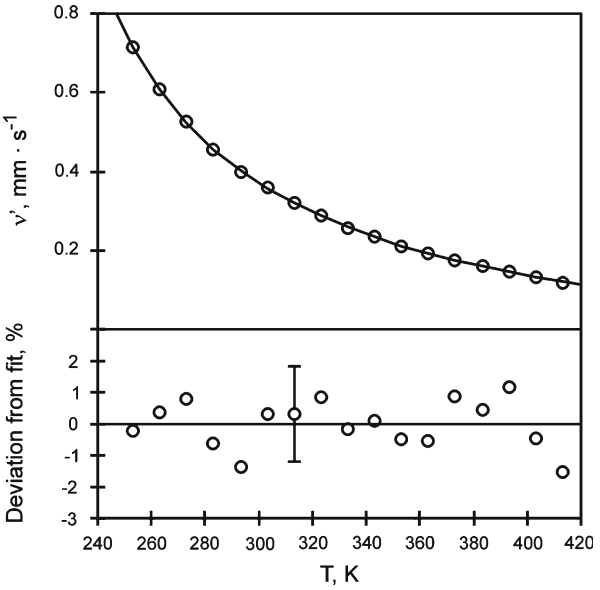

Fig. 11. Liquid kinematic viscosity ν' of SES36 under saturation conditions.

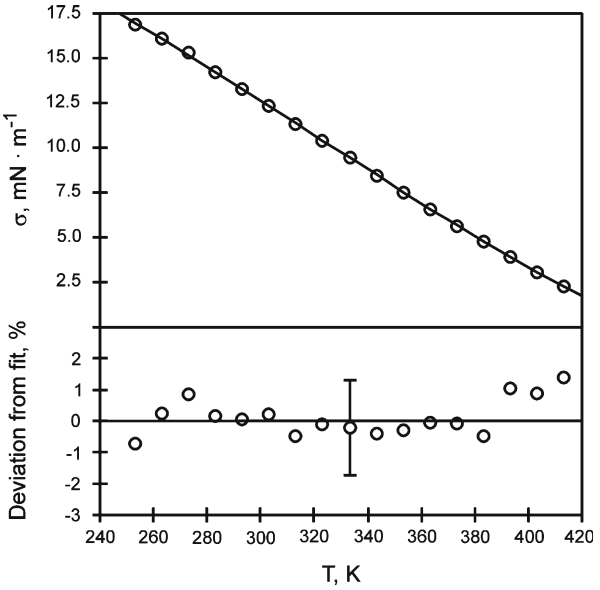

Fig. 12. Surface tension σ of SES36 under saturation conditions.

Table XI. Coefficients of Eq. (16)

ν'_0 ($mm^2 \cdot s^{-1}$)	1371
ν'_1 (K)	-2295.36
ν'_2 (K^{-1})	-0.01369
ν'_3 (K^2)	318,784
rms (%)	0.74
T-range (K)	253 – 413

Table XII. Coefficients of Eq. (17)

σ_0 ($mN \cdot m^{-1}$)	41.93
σ_1	1.188
σ_2	−1.462
rms (%)	0.59
T-range (K)	253–413

the form,

$$\nu' = \nu'_0 \exp\left[\nu'_1 T^{-1} + \nu'_2 T + \nu'_3 T^{-2}\right] \tag{16}$$

in order to represent the kinematic viscosity of SES36, where T is the temperature in K and the coefficients are given in Table XI. Here, also the standard deviation of our data relative to those calculated by Eq. (16) is reported. It should be noted that the residuals of the experimental data from the fit are smaller than the standard deviations of the individual measurements, which were in most cases smaller than 1.0%.

The experimental data for the surface tension can be well represented by a modified van der Waals-type surface tension equation of the form [30],

$$\sigma = \sigma_0 (1 - T_R)^{1.26} \left[1 + \sigma_1 (1 - T_R)^{0.5} + \sigma_2 (1 - T_R)\right], \tag{17}$$

where the fit parameters σ_0, σ_1, and σ_2 are given in Table XII. The present correlation, Eq. (17), represents the experimental values of the surface tension with a root-mean-square deviation of about 0.6%.

4. CONCLUSIONS

The present work presents a comprehensive characterization of SES36, a newly developed multicomponent refrigerant mixture. In addition to measurements of the vapor pressure ($304\,K < T < 448\,K$; $\Delta p_S \approx \pm 2\,kPa$),

saturated-liquid densities ($273\,\mathrm{K} < T < 363\,\mathrm{K}$; $\Delta\rho/\rho \approx \pm 0.1\%$), compressed-liquid densities ($373\,\mathrm{K} < T < 448\,\mathrm{K}$; $p_\mathrm{S} < p < 4.5\,\mathrm{MPa}$; $\Delta\rho/\rho \approx \pm 0.3\%$), and superheated-vapor densities ($348\,\mathrm{K} < T < 448\,\mathrm{K}$; $0.1\,\mathrm{MPa} < p < p_\mathrm{S}$; $\Delta\rho/\rho \approx \pm 0.3$ to $\pm 3\%$) have been determined using a vibrating-tube method. Light scattering from bulk fluids has been successfully applied for the determination of the thermal diffusivity ($\Delta a/a \approx \pm 2.0\%$) and sound speed ($\Delta u_\mathrm{S}/u_\mathrm{S} \approx \pm 0.5\ \%$) in the liquid and vapor phases under saturation conditions, from 293 K approaching the critical point. In addition, the sound speed has been obtained for the superheated-vapor region ($393\,\mathrm{K} < T < 523\,\mathrm{K}$; $0.5\,\mathrm{MPa} < p < 2.5\,\mathrm{MPa}$; $\Delta u_\mathrm{S}/u_\mathrm{S} \approx \pm 0.5\%$). Applying surface light scattering on the phase boundary between liquid and vapor SES36, its liquid kinematic viscosity ($\Delta\nu/\nu \approx \pm 1.5\%$) and surface tension ($\Delta\sigma/\sigma \approx \pm 1.5\%$) have been determined under saturation conditions ($253\,\mathrm{K} < T < 413\,\mathrm{K}$). By combining the experimental data obtained by the different measurement techniques, the critical-point parameters ($T_\mathrm{C} = 450.7 \pm 0.5\,\mathrm{K}$; $p_\mathrm{C} = 2.849 \pm 0.024\,\mathrm{MPa}$; $\rho_\mathrm{C} = 538 \pm 16\,\mathrm{kg \cdot m^{-3}}$) have been derived.

This first insight into the thermophysical properties of SES36, whose azeotropic behavior was checked, allows calculation of all equilibrium gas-phase thermodynamic properties and several thermodynamic functions of the saturated liquid for engineering practice. Due to the relatively less accurate values for the density in the superheated region and lacking sound-speed data at low pressures, at present, this can be attained only by the combination of experimental data with prediction methods, e.g., for calculation of the third virial coefficient and the ideal-gas heat capacity. While the present work summarizes more or less all of our experimental investigations, in future work we will focus on derived thermodynamic data for SES36. Here, data for the density and sound speed at low pressures obtained by other techniques and/or research groups, may be the most helpful.

ACKNOWLEDGMENT

We thank Cristina Botero for her valuable assistance in carrying out many of the light scattering experiments.

REFERENCES

1. *REFPROP Standard Reference Database 23*, Version 7.1 (Nat. Inst. Stds. Technol., Gaithersburg, MD, 2003).
2. B. J. Berne and R. Pecora, *Dynamic Light Scattering* (Robert E. Krieger, Malabar, 1990).
3. B. Chu, *Laser Light Scattering* (Academic Press, New York, 1991).

4. J. N. Shaumeyer, R. W. Gammon, and J. V. Sengers, in *Measurement of the Transport Properties of Fluids*, W. A. Wakeham, A. Nagashima, and J. V. Sengers, eds. (Blackwell Scientific, Oxford, 1991), pp. 197–213.
5. A. Leipertz and A. P. Fröba, in *Diffusion in Condensed Matter – Methods, Materials, Models*, P. Heitjans and J. Kärger, eds. (Springer, Berlin, 2005), pp. 583–622.
6. A. Bardow, *Fluid Phase Equilib.* **251**:121 (2007).
7. G. Wu, M. Fiebig, and A. Leipertz, *Int. J. Heat Mass Transfer* **31**:1471 (1988).
8. A. Leipertz, *Chem. Ing. Tech.* **64**:17 (1992).
9. S. Will, A. P. Fröba, and A. Leipertz, *Int. J. Thermophys.* **19**:403 (1998).
10. A. P. Fröba, S. Will, and A. Leipertz, *Fluid Phase Equilib.* **161**:337 (1999).
11. D. Langevin, *Light Scattering by Liquid Surfaces and Complementary Techniques* (Marcel Dekker, New York, 1992).
12. A. P. Fröba, *Simultane Bestimmung von Viskosität und Oberflächenspannung transparenter Fluide mittels Ober-flächenlichtstreuung*, Dr.-Ing. thesis, Friedrich-Alexander-Universität Erlangen-Nürnberg, Erlangen (2002).
13. E. H. Lucassen-Reynders and J. Lucassen, *Adv. Colloid Interface Sci.* **2**:347 (1969).
14. A. P. Fröba and A. Leipertz, *Int. J. Thermophys.* **24**:895 (2003).
15. I. M. Marrucho, N. S. Oliveira, and R. Dohrn, *J. Chem. Eng. Data* **47**:554 (2002).
16. A. P. Fröba, K. Krzeminski, and A. Leipertz, *Int. J. Thermophys.* **25**:987 (2004).
17. W. Wagner, *Eine mathematisch statistische Methode zum Aufstellen thermodynamischer Gleichungen - gezeigt am Beispiel der Dampfdruckkurve reiner-fluider Stoffe*, Fortschrittsberichte der VDI-Zeitschrift, Reihe 3, Nr. 39 (VDI-Verlag, Düsseldorf, 1974).
18. K. S. Pitzer, *J. Am. Chem. Soc.* **77**:3427 (1955).
19. K. S. Pitzer, D. Z. Lippmann, R. F. Curl, C. M. Huggins, and D. E. Peterson, *J. Am. Chem. Soc.* **77**:3433 (1955).
20. L. A. Weber, *Int. J. Thermophys.* **15**:461 (1994).
21. D. X. Liu and H. W. Xiang, *Int. J. Thermophys.* **24**:1667 (2003).
22. H. W. Xiang, *Chem. Eng. Sci.* **57**:1439 (2002).
23. R. D. Gunn and T. Yamada, *AIChE J.* **17**:1341 (1971).
24. Z.-S. Chen and T. Ito, *Proc. 5th Asian Thermophys. Props. Conf.* (Seoul, 1998), pp. 321–323.
25. P. Hu and Z.-S. Chen, *Fluid Phase Equilib.* **221**:7 (2004).
26. K. Kraft, M. M. Lopes, and A. Leipertz, *Int. J. Thermophys.* **16**:423 (1995).
27. K. G. Joback, *A Unified Approach to Physical Property Estimation Using Multivariate Statistical Techniques,* M.Sc. Thesis, Massachusetts Institute of Technology, Cambridge, MA, 1984.
28. R. C. Reid, J. M. Prausnitz, and B. E. Poling, *The Properties of Gases and Liquids* (McGraw-Hill, New York, 1977 and 1987).
29. K. Lucas, *Chem. Ing. Tech.* **46**:157 (1974).
30. C. Miqueu, D. Broseta, J. Satherley, B. Mendiboure, J. Lachaise, and A. Graciaa, *Fluid Phase Equilib.* **172**:169 (2000).